Published in final edited form as:
Vis Neurosci. 2006 ; 23(1): 11–24. doi:10.1017/S095252380623102X.

The *nob2* mouse, a null mutation in *Cacna1f*: Anatomical and functional abnormalities in the outer retina and their consequences on ganglion cell visual responses

BO CHANG[1], **JOHN R. HECKENLIVELY**[2,3], **PHILIPPA R. BAYLEY**[4], **NICHOLAS C. BRECHA**[2,5,6], **MURIEL T. DAVISSON**[1], **NORM L. HAWES**[1], **ARLENE A. HIRANO**[2,5,6], **RONALD E. HURD**[1], **AKIHIRO IKEDA**[7], **BRITT A. JOHNSON**[7], **MAUREEN A. MCCALL**[8,9], **CATHERINE W. MORGANS**[4], **STEVE NUSINOWITZ**[2], **NEAL S. PEACHEY**[10,11], **DENNIS S. RICE**[12], **KIRSTAN A. VESSEY**[8], and **RONALD G. GREGG**[9,13]

[1]The Jackson Laboratory, Bar Harbor, Maine

[2]Jules Stein Eye Institute, University of California at Los Angeles, Los Angeles, California

[3]W.K. Kellogg Eye Center, University of Michigan, Ann Arbor, Michigan

[4]Neurological Sciences Institute, Oregon Health and Science University, Beaverton, Oregon

[5]Departments of Neurobiology and Medicine, Geffen School of Medicine, University of California at Los Angeles, Los Angeles, California

[6]Research Service, VAGLAHS, Los Angeles, California

[7]Department of Genetics, University of Wisconsin, Madison, Wisconsin

[8]Department of Psychological and Brain Sciences, University of Louisville, Louisville, Kentucky

[9]The Center for Genetics and Molecular Medicine, University of Louisville, Louisville, Kentucky

[10]Research Service, Cleveland VAMC, Cleveland, Ohio

[11]Cole Eye Institute, Cleveland Clinic Foundation, Cleveland, Ohio

[12]Lexicon Genetics, The Woodlands, Texas

[13]Department of Biochemistry and Molecular Biology, University of Louisville, Louisville, Kentucky

Abstract

Glutamate release from photoreceptor terminals is controlled by voltage-dependent calcium channels (VDCCs). In humans, mutations in the *Cacna1f* gene, encoding the α_{1F} subunit of VDCCs, underlie the incomplete form of X-linked congenital stationary night blindness (CSNB2). These mutations impair synaptic transmission from rod and cone photoreceptors to bipolar cells. Here, we report anatomical and functional characterizations of the retina in the *nob2* (*no b-wave 2*) mouse, a naturally occurring mutant caused by a null mutation in *Cacna1f*. Not surprisingly, the *b*-waves of both the light- and dark-adapted electroretinogram are abnormal in *nob2* mice. The outer plexiform layer (OPL) is disorganized, with extension of ectopic neurites through the outer nuclear layer that originate from rod bipolar and horizontal cells, but not from hyperpolarizing bipolar cells. These ectopic neurites continue to express mGluR6, which is frequently associated with profiles that label with the

Address correspondence and reprint requests to: Neal S. Peachey, Cole Eye Institute (I-31), Cleveland Clinic Foundation, Cleveland, OH 44106, USA. peachen@ccf.org.

presynaptic marker Ribeye, indicating potential points of ectopic synapse formation. However, the morphology of the presynaptic Ribeye-positive profiles is abnormal. While cone pedicles are present their morphology also appears compromised. Characterizations of visual responses in retinal ganglion cells *in vivo*, under photopic conditions, demonstrate that ON-center cells have a reduced dynamic range, although their basic center-surround organization is retained; no alteration in the responses of OFF-center cells was evident. These results indicate that *nob2* mice are a valuable model in which to explore the pathophysiological mechanisms associated with *Cacna1f* mutations causing CSNB2, and the subsequent effects on visual information processing. Further, the *nob2* mouse represents a model system in which to define the signals that guide synapse formation and/or maintenance in the OPL.

Keywords

Bipolar and horizontal cells; Congenital stationary night blindness; Electroretinogram; ON- and OFF-pathways; Voltage-dependent calcium channel

Introduction

Rod and cone photoreceptors synapse with second-order retinal neurons in a specialized plexus known as the outer plexiform layer (OPL). In darkness, rods and cones release the neurotransmitter, glutamate, at a continuous rate (Copenhagen & Jahr, 1989; Massey, 1990). Light induces hyperpolarization of photoreceptors, slows calcium influx through voltage-dependent calcium channels (VDCCs), thereby reducing the rate of glutamate release (Schmitz & Witkovsky, 1997). Disruptions in this process reduce the efficacy of synaptic transfer of the light response from photoreceptors to the second-order retinal neurons, the bipolar and horizontal cells. This can be evaluated noninvasively with the electroretinogram (ERG). When only synaptic transmission is compromised, the *a*-wave component, reflecting activity of rod and cone photoreceptors (Lamb, 1996), is spared, while the *b*-wave, reflecting predominantly rod or cone depolarizing bipolar cell (DBC) activity (Robson & Frishman, 1995, 1998; Kofuji et al., 2000; Sharma et al., 2005), is reduced. This “negative” ERG pattern has now been reported in mice with mutations in genes encoding mGluR6 (Masu et al., 1995), nyctalopin (Pardue et al., 1998), the G-protein subunit $G\alpha_{O1}$ (Dhingra et al., 2000, 2002), the β_2 subunit of VDCCs (Ball et al., 2002), the presynaptic cytomatrix protein bassoon (Dick et al., 2003), or calcium-binding protein 4 (Haeseleer et al., 2004). The wide variety of proteins essential for normal synaptic transmission is suggestive of the intricacy of the synaptic complex linking photoreceptors and DBCs.

In humans, negative ERGs have been observed in two forms of X-linked congenital stationary night blindness (CSNB; Miyake et al., 1986). The incomplete form, CSNB2, is caused by mutations in the *Cacna1f* gene, encoding the α_{1F} subunit of VDCCs (Bech-Hansen et al., 1998; Strom et al., 1998; Boycott et al., 2001; Wutz et al., 2002). In the outer retina, expression of the α_{1F} subunit has been localized to the OPL where it is concentrated on the presynaptic side in the terminals of the photoreceptors at their “active zones,” which are specialized to mediate continuous calcium-dependent neurotransmitter release (Morgans et al., 2001).

Here we describe the identification and characterization of a mouse with a spontaneous loss-of-function mutation in the *Cacna1f* gene. Affected mice have ERG abnormalities that are similar to those observed in CSNB2 patients, and have been named *nob2* (*no b-wave 2*). In the *nob2* retina, synaptic structures in the OPL are disorganized and horizontal and rod bipolar cells extend ectopic neurites into the outer nuclear layer (ONL) and beyond. In spite of this extensive dendritic remodeling, retinal ganglion cell (RGC) receptive fields are normal at photopic adaptation levels, although changes in spontaneous and light-evoked activity are seen

in ON-center cells. Our results indicate that the *nob2* mouse is a new model of CSNB2 and should provide insight into the pathophysiological processes associated with this disorder in humans and the subsequent effect of these abnormalities on visual processing. Further, the *nob2* mouse can be used to explore the role of presynaptic calcium influx and neurotransmitter release in ribbon synapse development.

Materials and methods

Animals

Wild-type (WT) and *nob2* mice used in this study were obtained from The Jackson Laboratory (Bar Harbor, ME), either directly or as the progeny from breeders shipped to the institutions involved. In some experiments, we also studied *nob* mice, which have a mutation in the *nyx* gene and are a model of complete CSNB (CSNB1; Pardue et al., 1998; Gregg et al., 2003*a*). *nob* mice were generated in a breeding colony maintained at the Cleveland VA Medical Center. In all facilities, mice were maintained on a 12-h light/12-h dark cycle and were provided food and water *ad libitum*. All of the experiments that assessed the visual response properties of RGCs were conducted at the University of Louisville. All procedures involving animals were approved by the individual institute's Institutional Animal Care and Use Committee and were conducted in accordance with the Institute for Laboratory Animal Research Guide for Care and Use of Laboratory Animals.

Positional cloning

The *nob2* mouse was initially identified in a recombinant inbred strain, AXB6, established between A/J and C57BL/6J strains (AXB6/PgnJ) and maintained at the Jackson Laboratory. *nob2* was discovered as part of an ERG-based screen for spontaneous retinal mutants (Chang et al., 2002). All other recombinant inbred strains from the panels (AXB, BXA) had normal *b*-waves, indicating that the defect in *nob2* was the result of a rare spontaneous mutation in the AXB6 line. To determine the chromosomal location of the *nob2* gene, affected AXB6 mice were crossed to CAST/EiJ mice. When male *nob2* mice were used, all F1 mice were unaffected, consistent with a recessive inheritance pattern. When female *nob2* mice were mated to CAST/EiJ males, all F1 female offspring had normal ERGs, while all F1 male offspring were affected, indicating that *nob2* was an X-linked trait. For genetic mapping, F1 *nob2*/CAST/EiJ females were crossed to CAST/EiJ males. The phenotype of a total of 200 F2 male mice was determined by ERG recording and these mice were genotyped using microsatellite markers across the X chromosome.

Polymerase chain reaction (PCR) genotyping

DNA was isolated from tail snips as previously reported (Buffone & Darlington, 1985). For PCR amplification, 25 ng DNA was used in a 10-μl volume containing 50 mM KCl, 10 mM Tris-HCl, pH 8.3, 2.5 mM $MgCl_2$, 0.2 mM oligonucleotides, 200 μM dNTPs, and 0.02 U AmpliTaq DNA polymerase. The reactions were initially denatured for 3 min at 94°C, and then subjected to 40 cycles of 15 s at 94°C, 1 min at 51°C, 1 min at 72°C, and a final 7-min extension at 72°C. PCR products were separated by electrophoresis on 3% MetaPhor (FMC, Rockland, ME) agarose gels, stained with ethidium bromide, and visualized under UV light. Initially a scan of the X chromosome using microsatellite (Mit) DNA markers was carried out on pooled DNA samples (Taylor et al., 1994). After detection of linkage on the X chromosome, microsatellite markers were scored on individual DNA samples. To test the *Cacna1f* gene as a candidate, four pairs of PCR primers were used to amplify the entire open reading frame of the gene from cDNA. PCR products were sequenced directly using standard fluorescent-based sequencing methods. Total RNA was isolated from retinas of newborn mice using TRIZOL LS Reagent (Invitrogen Life Technologies, Carlsbad, CA) and the SuperScript™ preamplification system (Invitrogen Life Technologies) was used to synthesize first strand

cDNA. The genomic DNA fragment containing the transposon insertion in exon 2 that is illustrated in Fig. 1a and flanking DNA was amplified using the Accuprime DNA polymerase as described by the manufacturer (Invitrogen Life Technologies). The PCR fragment containing the transposon insertion was sequenced by fluorescent cycle sequencing.

Histology

Mice were killed by CO_2 administration and the eyes were removed and immersion fixed overnight. For light microscopy the eyes were fixed at 4°C in Bouin's fixative, rinsed in phosphate-buffered saline, dehydrated, and embedded in paraffin. Sections 6-μm thick were cut on a RM 2135 microtome (Leica Microsystems, Wetzlar, Germany), mounted onto slides, rehydrated, and stained using hematoxylin and eosin.

Preparation of retinal sections for immunohistochemistry

Mouse eyecups or isolated retinas were prepared as described previously (McCall et al., 2002). Freshly dissected eyecups or retinas were fixed for 5–60 min by immersion in 4% (w/v) paraformaldehyde in 0.1 M phosphate buffer, pH 7.4 (PB). They were then washed in PB, cryoprotected through a graded sucrose series, and frozen in OCT-20% sucrose (2:1) (Barthel & Raymond, 1990; Sakura Finetek, Torrance, CA). Sections 18-μm-thick were cut on a cryostat, mounted onto Super-Frost glass slides, air-dried, and stored at −80°C until used.

Immunofluorescent staining

Sections were brought to room temperature, and incubated in a blocking solution [5% (v/v) normal horse serum, 0.5% (v/v) Triton X-100 in PB] for 30 min. This solution was replaced and sections were incubated with primary antibody diluted in blocking solution for either 1–2 h at room temperature or overnight at 4°C. Primary antibodies and dilutions were as follows: monoclonal anti-α_{1F} (4G2; Morgans et al., 2005, at 1:2); anti-Ctbp2/Ribeye (BD Biosciences Pharmingen, San Diego, CA, at 1:5000); anti-Protein Kinase Cα (PKC; Sigma, St Louis, MO, at 1:5000); anti-calbindin D-28K (Chemicon, Temecula, CA, at 1:1000); anti-Neurokinin-3 receptor (NK3R; Grady et al., 1996, at 1:500); rhodamine-labeled PNA (Vector Labs, Burlingame, CA, at 1 μg/ml); and anti-mGluR6 (Neuromics, Minneapolis, MN, at 1:1000). After washing in PB three times for 20 min, sections were incubated in fluorescent secondary antibodies at room temperature for 1 h. Secondary antibodies were: 1:500 dilution of CY3 conjugated goat anti-mouse (Jackson ImmunoResearch, West Grove, PA) for α_{1F}; 1:1000 dilution of Alexa 488 conjugated goat anti-mouse (Ribeye); and 1:1000 dilution of Alexa 488 or Alexa 568 goat anti-rabbit (mGluR6, PKC, calbindin, NK3R; Invitrogen Life Technologies, Carlsbad, CA). Slides were washed three times in PB and then coverslipped with Crystal/Mount mounting medium (Biomeda, Foster City, CA). Immunostained sections were imaged on either a Zeiss LSM 510 META or an Olympus FV300 confocal microscope. Images presented are all maximum projections of stacks of confocal sections, adjusted for contrast and brightness with Adobe Photoshop.

Electroretinography

After overnight dark adaptation, mice were anesthetized with ketamine (80 mg/kg) and xylazine (16 mg/kg). Eye drops were used to anesthetize the cornea (1% proparacaine HCl) and to dilate the pupil (1% mydriacyl, 2.5% phenylephrine HCl, 1% cyclopentolate HCl). Mice were placed on a temperature-regulated heating pad throughout the recording session.

ERGs were recorded using a stainless-steel electrode that was coiled in a small loop and made contact with the corneal surface through a thin layer of 0.7% methylcellulose. Needle electrodes placed in the cheek and the tail served as reference and ground leads, respectively. Responses were differentially amplified (0.05–1500 Hz), averaged, and stored using a UTAS E-3000

signal averaging system (LKC Technologies, Gaithersburg, MD). Stimulus flashes were first presented to the dark-adapted eye, and ranged in intensity from −3.6 log cd s/m^2 to 2.1 log cd s/m^2. Stimuli were presented in order of increasing intensity. The number of successive responses averaged together decreased from 20 for low-intensity flashes to 2 for the highest intensity stimuli. The duration of the interstimulus interval (ISI) increased from 4 s for low-intensity flashes to 90 s for the highest intensity stimuli. A steady rod-desensitizing adapting field was then presented within the ganzfeld bowl. After allowing a 7-min period of light adaptation, cone ERGs were recorded to flashes superimposed upon an adapting field. Flash intensity ranged from −0.8 log cd s/m^2 to 1.9 log cd s/m^2 and responses to 100 flashes presented at 2.1 Hz were averaged at each intensity level.

The major components of the ERG were measured conventionally. The amplitude of the *a*-wave was measured from the prestimulus baseline to the *a*-wave trough. The amplitude of the *b*-wave was measured from the *a*-wave trough to the peak of the *b*-wave or, if no *a*-wave was present, from the prestimulus baseline. The implicit time of the *b*-wave was measured from the time of flash presentation to the peak of the *b*-wave. To derive Rm_{P3}, representing the maximum *a*-wave amplitude, the leading edge of the dark-adapted *a*-wave was fitted with a model of rod phototransduction (Pugh & Lamb, 1993), as described elsewhere (Nusinowitz et al., 2003).

Extracellular in vivo single-unit retinal ganglion cell recording

Visual responses were recorded extracellularly from the optic nerve of WT and *nob2* mice, *in vivo*, under photopic conditions, using previously published procedures (Sagdullaev & McCall, 2005). Mice were anesthetized with ketamine (127 mg/ml) and xylazine (12 mg/ml), and anesthesia was maintained throughout the course of the experiment with hourly supplemental injections of the original dose diluted to 42%. Mice were placed in a stereotaxic (David Kopf Instruments, Tujunga, CA) and body temperature was maintained at 37°C with a thermostat-controlled heating pad (CWE Instruments, Ardmore, PA). Eyedrops (1% mydriacyl, 2.5% phenylephrine HCl) were used to dilate the right pupil and to paralyze accommodation and a clear, plano, plastic contact lens (Sagdullaev et al., 2004) was placed over each eye to prevent corneal drying. A small craniotomy was performed and the cortex overlying the optic nerve was removed using vacuum suction. Tungsten electrodes (40–70 MΩ impedance) were inserted into the optic nerve and a reference electrode was inserted into the skin on the back of the neck. Action potentials from single RGC axons were isolated, amplified (X3+Cell, slope/height window discriminator/amplifier, FHC, Bowdoinham, ME) and digitized at 21 kHz (Power1401, Cambridge Electronics Design, Cambridge, UK). Ganglion cell responses were played in real time over an audiomonitor (AM7, Grass Instruments, Quincy, MA) and displayed on both an oscilloscope (Tektronix 2215, Richardson, TX) and a computer monitor, and stored for future analysis using Spike2 software (Cambridge Electronic Design, Cambridge, UK).

The receptive-field center of each isolated RGC was mapped onto a tangent screen positioned between 10–20 cm from the mouse's eye using a handheld Pantoscope (Keeler Instruments, Broomall, PA). Once the sign and extent of the receptive-field center was determined, a Ganzfeld stimulator (Advanced Illumination, Rochester, VT), which contained 64 light emitting diodes and whose size could be adjusted with an iris diaphragm (Edmund Industrial Optics, Barrington, NJ), replaced the tangent screen and the aperture was adjusted to be slightly smaller than the size of the cell's receptive-field center. A computer program, Superscope II 2.17.1 (GW Instruments Inc., Somerville, MA) was used to synchronize stimulus presentation and response acquisition (Power1401, Cambridge Electronic Design).

After a 2-min adaptation period to a 30-cd/m^2 spot, each RGC was stimulated with a spot of optimal size and fixed duration (4s) whose intensity changed. For ON-center cells, the spot intensity increased in 0.25–0.5 log intensity steps from the adaptation level to 1680 cd/m^2. For

OFF-center cells the intensity decreased similarly from the adaptation level to 0 cd/m^2. Between the stimuli the screen returned to 30 cd/m^2. The duration of the ISI needed to maintain responses independent of the preceding stimulus was empirically determined and ranged from 10 s for the smallest intensity steps to 60 s for the largest intensity steps. Table 1 shows the exact intensities and ISIs for both increments and decrements. To account for differences in the total number of spikes that occur between transient and sustained RGC responses, the mean spike rate over the first 0.5 s after stimulus onset was used as a metric of the cell's response. For each RGC studied, the background firing rate was measured as the mean firing rate over 10 s after a 2-min adaptation period and prior to the presentation of the stimuli. This background rate was subtracted from each of the visually evoked responses. To compare across cells with different peak firing rates, responses were normalized relative to the maximum response for that cell. Responses were plotted against log (normalized intensity) for ON-center cells and −log (normalized intensity) for OFF-center cells, where normalized intensity is the ratio of stimulus intensity to the intensity of the adapting spot (30 cd/m^2). A Hill equation was fit to each data set (GraphPad Prism 4.03, San Diego, CA), and the semisaturation constant (log EI_{50}) and the Hill exponent (h) parameters were derived.

Results

nob2 is caused by a mutation in the Cacna1f gene

The *nob2* mutation was mapped between the microsatellite markers, DXMit123 and DXMit124, a region that includes *Cacna1f*. Sequence analysis revealed an insertion of a transposable element (*Mus musculus* transposon ETn) in exon 2 of the *Cacna1f* gene (Fig. 1a). This insertion results in an out-of-frame insertion, which is predicted to produce a stop codon after synthesis of only 32 amino acids. In view of these results, *nob2* mice have been renamed *Cacna1f*^{nob2}. In this manuscript, however, affected mice will continue to be referred to simply as *nob2*, regardless of their gender (i.e., *Cacna1f*^{nob2}/*Cacna1f*^{nob2} or *Cacna1f*^{nob2}/*Y*). To examine whether the α_{1F} subunit protein was expressed in the *nob2* retina, we reacted retinal cross sections with an antibody against the C-terminal 177 amino acids of rat α_{1F}, which recognizes α_{1F} in the OPL and inner plexiform layer (IPL) of WT mice (Morgans et al., 2005). As can be seen in Fig. 1b, there is no expression of α_{1F} in either synaptic layer in the *nob2* retina, which confirms that this spontaneous mutation results in a null allele. As can be seen by comparing the hematoxylin and eosin-stained transverse retinal sections from WT and *nob2* (Fig. 1c), adult *nob2* mice exhibit a disorganized OPL. In contrast, the lamination pattern of the rest of the *nob2* retina appears normal, despite the absence of expression of the α_{1F} subunit in the IPL.

ERGs are abnormal in nob2 mice

To evaluate overall retinal function, ERGs were recorded to full-field flashes using stimulus conditions that isolated rod- or cone-driven activity (Pardue et al., 1998). The *b*-wave component, reflecting activity of rod DBCs (Kofuji et al., 2000), was reduced in dark-adapted ERGs from *nob2* mice (red traces, Fig. 2a) compared to those obtained from B6AF1/J WT controls (black traces, Fig. 2a) throughout the stimulus range. The *b*-wave was not abolished, however, as *nob2* responses were consistently more positive than those obtained from *nob* mice (blue traces, Fig. 2a) that completely lack a dark-adapted *b*-wave (Pardue et al., 1998). The *nob2* responses also included high-frequency oscillatory potentials superimposed upon the *b*-wave. While diminished in comparison to WT, the presence of oscillatory potentials in *nob2* ERGs provides additional evidence that light-evoked activity reaches the inner retina (Wachtmeister, 1998; McCall et al., 2002). The maximum amplitude of the initial cornea-negative *a*-wave, reflecting the light-induced closure of sodium channels along the rod outer segment (Lamb, 1996), was similar in all mice tested (Figs. 2a & 2b), which is consistent with the absence of photoreceptor degeneration in these mice (Fig. 1c; Pardue et al., 1998). Between

−1.2 and 0.0 log cd s/m^2, however, *a*-waves were actually larger in *nob2* and *nob* mice than in B6AF1/J WT mice. This apparent enhancement occurs because normally the *b*-wave component truncates the *a*-wave (Hood & Birch, 1992). In *nob2* mice, the implicit time of the dark-adapted ERG *b*-wave was delayed (Fig. 2c).

CSNB in humans is a nonprogressive disorder (Greenstein et al., 1988). Thus, we examined whether the dark-adapted ERG abnormalities of *nob2* mice also were stable and recorded ERGs at 3, 7, and 15 months of age. To compensate for the reduction in overall amplitude that occurs in older WT mice (Li et al., 2001), values are expressed as a percentage of the mean for age-matched WT mice recorded under the same conditions. At each age tested, the maximum *a*-wave amplitude, represented by the Rm_{P3} values, from *nob2* mice were not different from those of WT animals (Fig. 2d). In addition, the relative amplitude of the *nob2 b*-wave was diminished to the same extent at all ages examined (Fig. 2d).

The *nob2* mutation also affects the cone pathway. Light-adapted ERGs from *nob2* mice (red tracings in Fig. 3a) were consistently reduced in amplitude and had slower kinetics than those of B6AF1/J WT controls (black traces in Fig. 3a). In comparison to *nob* responses (blue traces in Fig. 3a), however, *nob2* responses were more positive and had faster kinetics. Although cone ERGs of *nob2* and *nob* mice had distinct waveforms, their overall peak-to-trough amplitudes were similar (Fig. 3b). The implicit time of the cone ERG *b*-wave was delayed in both *nob2* and *nob* mice, although the magnitude of this delay was less pronounced in *nob2* responses (Fig. 3c). These data predict that deficits should be expected within the ON-pathway, mediated by either rods or cones. Unfortunately, the rodent ERG cannot easily be used to predict whether this mutation affects the OFF-pathway (Sharma et al., 2005).

Anatomical abnormalities in nob2 mice

Since the ERG *b*-wave abnormalities of *nob2* mice are likely to reflect a synaptic defect between photoreceptors and DBCs, we examined the morphology of dendrites of these postsynaptic cells. On the postsynaptic side, DBC and horizontal cell dendrites form an invagination in each rod spherule or multiple invaginations in each cone pedicle. These invaginations are associated with pre-synaptic structures referred to as synaptic ribbons, which are thought to facilitate the constant release of glutamate that occurs in the dark (von Gersdorff, 2001). Because of the disorganization of the *nob2* OPL that we observed at the light-microscope level, we also examined the localization of specific elements in the presynaptic terminals using immunohistochemistry and confocal microscopy. To examine the morphology of the entire rod bipolar cell, we reacted retinal sections with antibodies to PKCα Fig. 4a). Similar to previous reports (Greferath et al., 1990; Haverkamp & Wässle, 2000), dendrites of WT rod bipolar cells terminate in short tufts uniformly in the OPL. In comparison, in *nob2* retina the rod bipolar cell dendrites extend beyond the OPL into the outer nuclear layer (ONL) and, in many cases reach the retinal pigment epithelium (Fig. 4b). To examine the structure of horizontal cells we reacted retinal sections with an antibody to calbindin (Peichl & Gonzalez-Soriano, 1994; Haverkamp & Wässle, 2000). In WT retinas, calbindin-positive horizontal cell processes define a dense layer within the OPL (Fig 4c). Inthe *nob2* retina, the horizontal cell dendrites, like those of bipolar cells, extend across the ONL to the retinal pigment epithelium (Fig. 4d). Careful examination of confocal images indicated that every rod bipolar and horizontal cell showed these ectopic dendrites. By comparison the inner retina of the *nob2* mouse appears qualitatively normal. The cell bodies of the rod bipolar and calbindin-positive amacrine cells are appropriately located in the inner nuclear layer (INL) of the *nob2* retina and their axon terminals and processes laminate normally within the IPL. To assess the status of a subset of cone hyperpolarizing bipolar cells (HBCs) in the *nob2* retina, we used an antibody against NK3R (Hirano & Brecha, 2002; Haverkamp et al., 2003). The dendritic arbors of this class of HBCs in the *nob2* mice are indistinguishable from WT (Figs. 4e & 4f). Thus, it appears

that the dendrites of the NK3R-positive HBCs are unaffected by the lack the α_{1F} in photoreceptors.

To better define alterations in the relationship between photoreceptors and second-order neurons, we examined the expression pattern of one postsynaptic (mGluR6) and two presynaptic markers [Ribeye and peanut agglutinin (PNA)] in transverse retinal sections. Ribeye (also referred to as Ctbp) is a component of the presynaptic ribbon complex and is present in both rod and cone terminals (Schmitz et al., 2000), whereas PNA recognizes cone photoreceptor terminals only (Blanks & Johnson, 1983). The postsynaptic marker, mGluR6, is expressed on the dendritic tips of both rod and cone DBCs (Masu et al., 1995; Sterling & Matthews, 2005). Figs. 5a and 5b show double labeling for Ribeye (green) and PNA (red) in the OPL of WT and *nob2* mice, respectively. In the WT retina, Ribeye is confined to the OPL and resembles a series of arcuate or horseshoe-shaped structures, typical of synaptic ribbon morphology (Schmitz et al., 2000; tom Dieck et al., 2005). In the *nob2* retina, Ribeye expression is altered significantly (Figs. 5b). Most horseshoe-shaped structures are missing from what remains of the OPL and are replaced by small diffuse punctate staining both in the residual OPL and throughout the ONL, where the bipolar and horizontal cells extend their ectopic processes. Cone terminals, as shown by PNA labeling, are restricted to the OPL in WT retina (Fig. 5a) and also to the residual OPL of the *nob2* retina (Fig. 5b). Inthe *nob2* retina, however, the pattern of PNA staining is disorganized (Fig. 5b), an effect that may be secondary to the gross disorganization of the OPL.

Figs. 5c–5f compare the expression patterns for Ribeye and PNA with that of the postsynaptic marker, mGluR6. In WT mice (Fig. 5c), mGluR6 puncta (red) align with the horseshoe-shaped structures defined by Ribeye (green) expression. In the *nob2* retina (Fig. 5d), however, the morphology of the Ribeye-positive profiles is altered and the overall density of structures stained for Ribeye and mGluR6 are reduced. While there remain cases in which a close apposition of staining between Ribeye and mGluR6 in *nob2* mice is maintained, this association is reduced compared to WT retina. It remains to be determined whether these associations represent ectopic synapses, as has been observed in *bassoon* knockout (KO) mice (Dick et al., 2003).

To determine if the dendrites of the cone DBCs colocalize with cone terminal profiles, we double labeled sections with an antibody to mGluR6 and with PNA. Fig. 5e shows a representative section through the OPL of a WT mouse retina. Both mGluR6 (red) and PNA (green) colocalize at the cone terminals (yellow); the additional punctate staining of mGluR6 represents rod bipolar cell dendritic tips. In the section from the *nob2* mouse, while cone terminals appear less organized, mGluR6-positive profiles continue to colocalize with cone terminals (Fig. 5f, yellow). Thus, both the ERG and morphological analyses point to a major disruption in the signaling patterns subserved by DBCs. In contrast, our morphological data suggest little impact on the cone-to-HBC pathway.

ON-center RGCs visual responses are altered in nob2 mice

Abnormalities in both rod- and cone-mediated vision have been documented in patients with CSNB1 and CSNB2 (Miyake et al., 1986), although quantitative characterizations of either central or peripheral vision have yet to be published. Our ERG results indicate that ON-pathway signaling through both rod and cone pathways should be compromised, while OFF cone pathway signaling might be spared. To compare the outcome of this potential alteration in signaling through the independent ON and OFF cone pathways, we examined basic receptive-field structure and visual response properties of RGCs in *nob2* mice under light-adapted conditions. Responses of 24 RGCs from *nob2* mice and 27 RGCs from WT mice were characterized by their responses to spots of light. Regardless of genotype, all RGCs could be classified as either ON-center (n = 13, 16; *nob2*, WT, respectively) or OFF-center (n = 11, 11;

nob2, WT, respectively). In addition, every RGC had a discrete receptive-field center that could be localized and mapped subjectively with hand-mapping techniques and there were no gross abnormalities evident between WT and *nob2* cells or when ON- and OFF-center cells were compared separately.

We determined both the spontaneous activity to a photopic adapting stimulus (30 cd/m^2) and the evoked activity to stimulus increments or decrements from that adaptation level for the same ON- and OFF-center RGCs in both WT and *nob2* mice. When we compared the spontaneous activity for ON-center cells, we found a significant difference between *nob2* and WT mice. The spontaneous activity of ON-center cells in *nob2* mice was less than half that in WT mice (14.8 ± 1.5 spikes/s *vs.* 31.6 ± 5.8 spikes/s; Student's *t*-test; $P = 0.017$). In contrast, spontaneous rates for OFF-center cells were similar between the two groups (*nob2 vs.* WT, 9.8 ± 1.6 spikes/s *vs.* 6.0 ± 1.7 spikes/s; Student's *t*-test; $P = 0.13$). These results suggest that steady state excitation through the ON-pathway is decreased in *nob2* mice compared to WT, whereas the cone-driven OFF-pathway remains unaffected. This is consistent with the reduced amplitude of the cone ERG *b*-wave throughout the range of intensities tested. To examine whether the range of intensities over which RGC responses could be evoked was also altered, we measured the responses of ON-center cells to optimally sized spots over a range of incremental stimuli increasing from the adapting level (30 cd/m^2) up to a maximum of 1680 cd/m^2. Similarly, responses of OFF-center cells were measured to decrements from the adapting level. Responses from a representative *nob2* ON-center RGC are shown in Fig. 6a. The normalized responses of the cells were plotted as a function of intensity to produce intensity–response functions. Mean response functions for all *nob2* ($n = 13$) and WT ($n = 16$) ON-center cells are compared in Fig. 6b. There is a significant decrease in the range of intensities over which ON-center RGCs in *nob2* mice can encode intensity changes. When a Hill equation was fit to the individual data sets, the intensity needed to reach a half-maximum response (log EI_{50}) was almost three times higher in WT than in *nob2* cells (log $EI_{50} = 0.86 \pm 0.14$ *vs.* 0.42 ± 0.03; ANOVA; $P = 0.004$). In addition, *nob2* ON-center cell responses saturated well before our highest intensity spot, an effect that we rarely observed in WT ON-center cells. These results indicate that the dynamic range and thus the ability of *nob2* ON-center cells to encode increments in intensity is dramatically reduced and predict that their increment thresholds would be significantly altered. In contrast, the intensity–response functions of OFF-center cells were similar in WT and *nob2* animals (log $EI_{50} = 0.47 \pm 0.04$ *vs.* 0.39 ± 0.03; ANOVA; $P > 0.05$; Fig. 6c). This differential affect on the ON-pathway of the *nob2* retina is consistent with the alterations seen in the ERG *b*-wave and in the propensity for second-order retinal neurons to develop ectopic neurites.

Discussion

We describe anatomical and functional changes in the retina of a mouse with a spontaneous mutation in the *Cacna1f* gene, which encodes the α_{1F} subunit (Cav1.4) of the VDCC. We show that the mutation is caused by the insertion of a transposon that results in a null allele and the absence of expression of this VDCC subunit protein in the retina. Similar to its manifestations in the human disease, ERG *b*-waves are significantly reduced under both dark- and light-adapted conditions, while *a*-waves are unaffected. This indicates that the primary defect in both mouse and human resides in altered synaptic transmission from both rods and cones to DBCs. In addition to this defective signal transmission, the dendrites of the rod DBCs and horizontal cells in *nob2* mouse retinas extend ectopic processes throughout the outer retina, which leads to the collapse of the OPL. In contrast, at least one class of HBCs are unaffected. In spite of these significant changes in the structure and function of the outer retina and an absence of expression of the α_{1F} subunit in the inner retina, visual responses and receptive fields of RGCs in the light-adapted *nob2* retinas exhibit relatively minor changes and those are limited to the ON-center RGCs.

The role of the α_{1F} subunit of the VDCCs in retinal synaptic transmission

Expression studies in heterologous systems show that α_{1F} combines with β and α_2/δ subunits to form functional L-type VDCCs (Koschak et al., 2003; Baumann et al., 2004; McRory et al., 2004; Hoda et al., 2005; Morgans et al., 2005). In the outer retina, the α_{1F} subunit of the VDCC is expressed in the OPL, and it has been localized specifically to both rod and cone photoreceptor terminals (Morgans et al., 2005). These data, and the fact that the α_{1F} subunit is critical to producing a VDCC on photoreceptor terminals that does not inactivate during sustained depolarization (Taylor & Morgans, 1998), indicate that this subunit may be the primary VDCC α_1 subunit involved in mediating tonic glutamate release from rods and cones. The results of the current study are concordant with this hypothesis. Under dark-adapted conditions, *nob2* mice exhibit a marked reduction in the ERG *b*-wave, while the *a*-wave component is spared. This indicates that in the absence of the α_{1F} subunit, photoreceptors are able to hyperpolarize in response to light but that there is a significant loss of transmission from photoreceptors to second-order neurons. The role of the α_{1F} VDCC subunit in the inner retina is less clear, although its expression is widespread. As in the outer retina, it would be expected to mediate glutamate release from the bipolar cells. The continued presence of high-frequency oscillatory potentials in the ERG indicates that function in the inner retina of *nob2* mice may be less compromised than in the outer retina in the absence of α_{1F}. Our characterization of visual responses and receptive fields in RGCs is consistent with this observation and could indicate the use of, or compensation by, another α_1 subunit in the inner retina.

Role of the α_{1F} subunit of the VDCC in synaptic development or maintenance in the outer retina

In WT retina, central DBC dendrites and flanking horizontal cell processes invaginate into the spherule of the rod photoreceptor. In cone pedicles, multiple invaginations form, each containing a similar triadic configuration. In contrast, HBCs make flat synapses with cone terminals outside of the invaginations (Haverkamp et al., 2003). In the mouse retina, the development of the invaginating synapses is established by P14 (Blanks et al., 1974). The early stages of synapse development appear to be genetically determined, although full maturation is thought to depend upon activity-dependent processes that occur after eye opening (Mumm et al., 2005). In the adult *nob2* retina, every rod bipolar and horizontal cell extends ectopic dendrites across a disrupted OPL into the ONL, and these processes sometimes reach the retinal pigment epithelium. In addition, the morphology of the Ribeye-positive arcuate forms, which characterize the ribbon in the pre-synaptic process (tom Dieck et al., 2005), is abnormal. Thus, it is highly unlikely that rod spherules contain conventional invaginating synapses, although electron microscopy will be required to definitively resolve this issue. Certainly, the apposition of these Ribeye-positive profiles with mGluR6-positive puncta in the ONL indicates the possibility of ectopic synapses. Whether these alterations are the result of abnormal synapse formation or failure of synapse maintenance also remains to be determined. By contrast, the mGluR6-positive puncta that reflect DBC synapses onto cone pedicles appear to be less affected. It is possible that another VDCC α_1 subunit may be expressed and support at least partial synapse formation with the cone pedicle. This idea is supported by reports of α_{1D} expression in cone terminals (Wilkinson & Barnes, 1996; Taylor & Morgans, 1998; Morgans, 1999, Morgans et al., 2001, 2005) and is consistent with the greater ERG *b*-wave deficit in mice lacking the VDCC β_2 subunit (Ball et al., 2002), the only VDCC β subunit known to be expressed in the OPL (Ball et al., 2004).

Two other mutant mice have been reported that alter neurotransmitter release from photoreceptors and exhibit abnormal bipolar cell dendritic morphology and reduced ERG *b*-waves. These mice involve the β_2 subunit of the VDCC (Ball et al., 2002; Gregg et al., 2002) or calcium-binding protein 4 (Haeseleer et al., 2004). Similar abnormalities also have been

noted in mice lacking expression of bassoon (Dick et al., 2003) as well as in mice that lack functional rod or cone photoreceptors (Claes et al., 2004). In comparison, mice with mutations in the postsynaptic proteins mGluR6, nyctalopin or $G_{\alpha 0}$, do not share these morphological abnormalities (Pardue et al., 2001; Ball et al., 2003; Masu et al., 1995; Tagawa et al., 1999; Dhingra et al., 2000, 2002).

One common feature of all presynaptic mutants is that they have decreased ERG *b*-waves most likely because of a reduction in glutamate release. Some, including *nob2* mice or mice lacking the VDCC β_2 subunit (Ball et al., 2002), clearly also have a decrease in calcium entry. In these mutants the abnormal calcium signaling could involve processes other than neurotransmitter release (Ghosh & Greenberg, 1995). For example, calcium influx can activate intracellular pathways, which can act locally at the synapse or mediate changes in nuclear gene transcription (Rosen et al., 1994; Ghosh & Greenberg, 1995; Curtis & Finkbeiner, 1999), processes that have the potential to alter cell surface molecules that may be critical to normal synapse formation. *In vitro* studies have presented a possible link between VDCCs and photoreceptor development in which VDCC blockade inhibits process outgrowth, varicosity formation, and vesicle protein synthesis in developing rods (Zhang & Townes-Anderson, 2002; Nachman-Clewner et al., 1999). These results indicate that the presence and/or activity of VDCCs is required for normal development and synapse formation and/or maintenance in the outer retina.

It is also possible that glutamate release is a key component guiding bipolar and horizontal cell neurites to the photoreceptor active zones. Neurotransmitters have been proposed to act as an activity-dependent signal during synaptic development and neuronal plasticity in the retina (Redburn & Rowe-Rendleman, 1996). In particular, glutamate has been shown to play a role in synaptic motility (Engert & Bonhoeffer, 1999; Maletic-Savatic et al., 1999; Wong et al., 2000; Wong & Wong, 2001) and in the growth and maintenance of dendritic spines (Passafaro et al., 2003). Glutamate may also cell-autonomously affect presynaptic development using local feedback loops through presynaptic α-amino-3-hydroxy-5-methylisoxazole-4-propionic acid (AMPA)/kainate-type receptors (Chang & De Camilli, 2001). This local feedback loop could affect the growth and/or maintenance of the photoreceptor terminal through neuronal activity, although the presence of such presynaptic glutamate receptors in adult mice is debated (see review by Yang, 2004) and their expression during development is unknown. Further studies are required to determine the contributions of abnormal glutamate release, intracellular calcium signaling, or absent VDCCs to the *nob2* phenotype.

Ganglion cell response properties in nob2 mice

Our ERG and anatomical characterizations of the *nob2* mouse retina indicate that the impact of this mutation on the rod and cone pathways should differ. By definition, patients with CSNB are night blind, but those with CSNB2 also show deficits at photopic levels (Miyake et al., 1986). In characterizing RGC visual responses, we focused on a comparison of signaling through the ON and OFF cone pathways. Our results indicate that center-surround organization is unaffected in *nob2* mice and that their receptive-field organization is similar to WT cells. When we compared the spontaneous activity and responses to changes in intensity, we found that *nob2* OFF-center cells were unaffected. In contrast, ON-center cells in *nob2* mice showed both lower spontaneous activity and a change in the gain of their response to incremental light stimuli that significantly narrowed their dynamic range. This deficit in the ON-center pathway is consistent with the reduction in the mouse cone ERG *b*-wave that is known to have a major contribution from cone DBCs (Sharma et al., 2005). In addition, our results may indicate that the invaginating synapses characteristic of the ON-pathway are more dependent on the presence of the α_{1F} subunit, while the flat synapse with HBCs may normally rely on another mechanism or substitute another α_1 subunit in the absence of α_{1F}. While the primary defect in visual processing must occur at the first synapse in the *nob2* retina, it should be noted that there

also could be a secondary effect of the absence of α_{1F} subunit expression in the inner retina. Several possible α_{1F} containing VDCC-dependent synapses in either the inner or outer retina could be involved in the changes that we report. Further dissection and characterization of light responses will be required to determine the sites and underlying mechanisms of action.

Comparable studies have been made of RGCs in the *nob* mouse (Gregg et al., 2003*b*,2005). While *nob* RGCs could be characterized as responding to the onset of either a bright or dark stimulus, their receptive fields show no evidence of center-surround organization (Gregg et al., 2005).

nob2 mice provide a model for human disease

CSNB2 is a human retinal disorder that also is caused by mutations within the *Cacna1f* gene (Bech-Hansen et al. 1998; Strom et al. 1998; Zeitz et al., 2005). While most CSNB disorders are the result of null mutations, some may actually increase calcium entry but reduce overall function by shifting the operating range (Hemara-Wahanui et al., 2005; Hoda et al., 2005). The ERG is commonly used to confirm a diagnosis of CSNB (Fishman et al., 2001). If the *nob2* mouse is an accurate model for CSNB2, then the ERG features of the mouse should match those of human patients. The results reported here indicate that they do. Under dark-adapted conditions, both *nob2* mice and CSNB2 patients exhibit a marked reduction in the ERG *b*-wave, while the *a*-wave component is spared. In both cases, the ERG results are stable across age, consistent with a nonprogressive disorder. While diminished, both the *b*-wave and high-frequency oscillatory potentials are retained in *nob2* mice and CSNB2 patients, indicating the retention of some inner retinal activity in the absence of α_{1F}. While there are important differences in the origins of the primate and mouse cone ERG (Sieving et al., 1994; Sharma et al., 2005), these responses also indicate the presence of inner retinal activity in the absence of α_{1F}. A recent publication has described a KO mouse for α_{1F} (Mansergh et al., 2005). Like the *nob2* mouse, α_{1F}-KO mice do not express the α_{1F} subunit protein in the OPL, have a thinner than normal OPL, and develop ectopic neurites from DBCs and horizontal cells. However, the functional deficits reported in α_{1F}-KO mice are more severe than those we report here for *nob2* mice. For example, cone-driven RGC responses are preserved in *nob2* mice, while in the α_{1F}-KO mice under similar stimulation conditions, light-evoked responses were not observed in the superior colliculus, which is a central target of RGCs. In addition, in α_{1F}-KO mice, cone ERGs were absent and under dark-adapted conditions the α_{1F}-KO *a*-wave was reduced and oscillatory potentials were absent. It is not clear if these functional abnormalities noted in the α_{1F}-KO mutant are stable across age. Nevertheless, these functional abnormalities appear to distinguish α_{1F}-KO mice from patients with CSNB2 and raise the possibility that the α_{1F}-KO mouse develops cone photoreceptor dysfunction or degeneration, a possibility discussed by Mansergh et al. (2005) and consistent with recent reports linking some *Cacna1f* mutations with progressive retinal disorders (Nakamura et al., 2003; Jalkanen et al., 2004; Hope et al., 2005).

In contrast, the phenotype of the *nob2* mouse is more consistent with the phenotype seen in CSNB2 patients. The changes observed in the *nob2* RGC function predict alterations in the peripheral vision of CSNB2 patients since the mouse retina has been considered in many important respects to resemble the primate retina outside of the fovea (Jeon et al., 1998). Currently, little is known about more complex visual phenotypes of CSNB2 patients, but our results would predict a deficit in vision mediated by the ON-center pathway under light-adapted conditions. In particular, our results would predict that CSNB2 patients would show significant deficits in increment, but not decrement thresholds and discriminations.

Our results also predict that CSNB2 patients will have a reduced OPL thickness, as well as ectopic bipolar and horizontal cell dendrites. Confirmation of these anatomical abnormalities will require examination of donor eyes from patients with CSNB2, although advances in optical coherence tomography may soon allow the status of the OPL to be visualized in the living

human eye (Wollstein et al., 2005). Human studies aside, further analysis of *nob2* mice are likely to contribute to our understanding of the pathophysiology of CSNB2 and synaptogenesis in the OPL of the retina.

Acknowledgments

We are grateful to Allison Crosby and Susan Eichholtz for excellent technical assistance. This work was supported by National Institutes of Health Grants R01EY04067 (N.C.B.), RR001183 (M.T.D.), R01EY012354 (R.G.G.), R01EY007758 (J.R.H.), R01EY014701 (M.A.M.), R01EY 014700 (C.W.M.), R01EY14465 (N.S.P.), R24EY15638 (N.S.P.), and awards from the Medical Research Service, Department of Veterans Affairs to N.C. Brecha (Merit Award; Senior Research Career Scientist) and to N.S. Peachey (Merit Award; Research Career Scientist).

References

Ball SL, McEnery M, Gregg RG. Voltage gated calcium channel subunit composition and distribution in the retina. Investigative Ophthalmology and Visual Science 2004;45 E-abstract 5423.

Ball SL, Pardue MT, McCall MA, Gregg RG, Peachey NS. Immunohistochemical analysis of the outer plexiform layer in the *nob* mouse shows no abnormalities. Visual Neuroscience 2003;20:267–272. [PubMed: 14570248]

Ball SL, Powers PA, Shin HS, Morgans CW, Peachey NS, Gregg RG. Role of the β_2 subunit of voltage-dependent calcium channels in the retinal outer plexiform layer. Investigative Ophthalmology and Visual Science 2002;43:1595–1603. [PubMed: 11980879]

Barthel L, Raymond PA. Improved method for obtaining 3 μm cryosections for immunocytochemistry. Journal of Histochemistry and Cytochemistry 1990;38:1383–1388. [PubMed: 2201738]

Baumann L, Gerstner A, Zong X, Biel M, Wahl-Schott C. Functional characterization of the L-type Ca^{2+} channel Cav1.4 from mouse retina. Investigative Ophthalmology and Visual Science 2004;45:708–713. [PubMed: 14744918]

Bech-Hansen NT, Naylor MJ, Maybaum TA, Pearce WG, Koop B, Fishman GA, Mets M, Musarella MA, Boycott KM. Loss-of-function mutations in a calcium-channel α_1-subunit gene in Xp11.23 cause incomplete X-linked congenital stationary night blindness. Nature Genetics 1998;19:264–267. [PubMed: 9662400]

Blanks JC, Adinolfi AM, Lolley RN. Synaptogenesis in the photoreceptor terminal of the mouse retina. Journal of Comparative Neurology 1974;156:81–93. [PubMed: 4836656]

Blanks JC, Johnson LV. Selective lectin binding of the developing mouse retina. Journal of Comparative Neurology 1983;221:31–41. [PubMed: 6643744]

Boycott KM, Maybaum TA, Naylor MJ, Weleber RG, Robitaille J, Miyake Y, Bergen AAB, Pierpont ME, Pearce WG, Bech-Hansen NT. A summary of 20 CACNA1F mutations identified in 36 families with incomplete X-linked congenital stationary night blindness, and characterization of splice variants. Human Genetics 2001;108:91–97. [PubMed: 11281458]

Buffone GJ, Darlington GJ. Isolation of DNA from biological specimens without extraction with phenol. Clinical Chemistry 1985;31:164–165. [PubMed: 3965205]

Chang B, Hawes NL, Hurd RE, Davisson MT, Nusinowitz S, Heckenlively JR. Retinal degeneration mutants in the mouse. Vision Research 2002;42:517–525. [PubMed: 11853768]

Chang S, De Camilli P. Glutamate regulates actin-based motility in axonal filopodia. Nature Neuroscience 2001;4:787–793.

Claes E, Seeliger M, Michalakis S, Biel M, Humphries P, Haverkamp S. Morphological characterization of the retina of the CNGA3(-/-)Rho(-/-) mutant mouse lacking functional cones and rods. Investigative Ophthalmology and Visual Science 2004;45:2039–2048. [PubMed: 15161873]

Copenhagen DR, Jahr CE. Release of endogenous excitatory amino acids from turtle photoreceptors. Nature 1989;341:536–539. [PubMed: 2477707]

Curtis J, Finkbeiner S. Sending signals from the synapse to the nucleus: Possible roles for CaMK, Ras/ERK, and SAPK pathways in the regulation of synaptic plasticity and neuronal growth. Journal of Neuroscience Research 1999;58:88–95. [PubMed: 10491574]

Dhingra A, Jiang M, Wang TL, Lyubarsky A, Savchenko A, Bar-Yehuda T, Sterling P, Birnbaumer L, Vardi N. Light response of retinal ON bipolar cells requires a specific splice variant of $G\alpha_O$. Journal of Neuroscience 2002;22:4878–4884. [PubMed: 12077185]

Dhingra A, Lyubarsky A, Jiang M, Pugh EN Jr. Birnbaumer L, Sterling P, Vardi N. The light response of ON bipolar neurons requires $G\alpha_O$. Journal of Neuroscience 2000;20:9053–9058. [PubMed: 11124982]

Dick O, tom Dieck S, Altrock WD, Ammermüller J, Weiler R, Garner CC, Gundelfinger ED, Brandstätter JH. The presynaptic active zone protein bassoon is essential for photoreceptor ribbon synapse formation in the retina. Neuron 2003;37:775–786. [PubMed: 12628168]

Engert F, Bonhoeffer T. Dendritic spine changes associated with hippocampal long-term synaptic plasticity. Nature 1999;399:66–70. [PubMed: 10331391]

Fishman, GA.; Birch, DG.; Holder, GE.; Brigell, MG. Electrophysiologic Testing in Disorders of the Retina, Optic Nerve and Visual Pathway. Second edition. American Academy of Ophthalmology; San Francisco, California: 2001.

Ghosh A, Greenberg ME. Calcium signaling in neurons: Molecular mechanisms and cellular consequences. Science 1995;268:239–247. [PubMed: 7716515]

Grady EF, Baluk P, Böhm S, Gamp PD, Wong H, Payan DG, Ansel J, Portbury AL, Furness JB, McDonald DM, Bunnett NW. Characterization of antisera specific to NK1, NK2, and NK3 neurokinin receptors and their utilization to localize receptors in the rat gastrointestinal tract. Journal of Neuroscience 1996;16:6975–6986. [PubMed: 8824334]

Greenstein VC, Hood DC, Siegel IM, Carr RE. A possible use of rod–cone interaction in congenital stationary nightblindness. Clinical Vision Sciences 1988;3:69–74.

Greferath U, Grünert U, Wässle H. Rod bipolar cells in the mammalian retina show protein kinase C-like immunoreactivity. Journal of Comparative Neurology 1990;301:433–442. [PubMed: 2262600]

Gregg RG, Lukasiewicz PD, Peachey NS, Sagdullaev BT, McCall MA. Nyctalopin is required for signaling through depolarizing bipolar cells in the murine retina. Investigative Ophthalmology and Visual Science 2003b;44 ARVO E-abstract 4180.

Gregg RG, McCall MA, Peachey NS. Bipolar specific expression of nyctalopin fusion gene rescues no *b*-wave phenotype in *nob* mice. Investigative Ophthalmology and Visual Science 2005;46 ARVO E-abstract 3554.

Gregg RG, Mukhopadhyay S, Candille SI, Ball SL, Pardue MT, McCall MA, Peachey NS. Identification of the gene and the mutation responsible for the *nob* (no *b*-wave) phenotype. Investigative Ophthalmology and Visual Science 2003a;44:378–384. [PubMed: 12506099]

Gregg RG, Read DS, Peachey NS, Pardue MT, McCall MA. Photoreceptor voltage dependent calcium channels but not bipolar cell activity is required for normal ribbon synapse formation. Investigative Ophthalmology and Visual Science 2002;43 ARVO E-abstract 831.

Haeseleer F, Imanishi Y, Maeda T, Possin DE, Maeda A, Lee A, Rieke F, Palczewski K. Essential role of Ca^{2+}-binding protein 4, a Cav1.4 channel regulator, in photoreceptor synaptic function. Nature Neuroscience 2004;7:1079–1087.

Haverkamp S, Ghosh KK, Hirano AA, Wässle H. Immunocytochemical description of five bipolar cell types of the mouse retina. Journal of Comparative Neurology 2003;455:463–476. [PubMed: 12508320]

Haverkamp S, Wässle H. Immunocytochemical analysis of the mouse retina. Journal of Comparative Neurology 2000;424:1–23. [PubMed: 10888735]

Hemara-Wahanui A, Berjukow S, Hope CI, Dearden PK, Wu SB, Wilson-Wheeler J, Sharp DM, Lundon-Treweek P, Clover GM, Hoda JC, Striessnig J, Marksteiner R, Hering S, Maw MA. A CACNA1F mutation identified in an X-linked retinal disorder shifts the voltage dependence of Cav1.4 channel activation. Proceedings of the National Academy of Sciences of the U.S.A 2005;102:7553–7558.

Hirano AA, Brecha NC. Expression of the neurokinin-3 (NK3) receptor in off-type cone bipolar cells in mouse retina. Investigative Ophthalmology and Visual Science 2002;43 ARVO E-abstract No. 736.

Hoda J-C, Zaghetto F, Koschak A, Striessnig J. Congenital stationary night blindness type 2 mutations S229P, G369D, L1068P, and W1440X alter channel gating or functional expression of $Ca_V1.4$ L-type Ca^{2+} channels. Journal of Neuroscience 2005;25:252–259. [PubMed: 15634789]

Hood DC, Birch DG. A computational model of the amplitude and implicit time of the *b*-wave of the human ERG. Visual Neuroscience 1992;8:107–126. [PubMed: 1558823]

Hope CI, Sharp DM, Hemara-Wahanui A, Sissingh JI, Lundon P, Mitchell EA, Maw MA, Clover GM. Clinical manifestations of a unique X-linked retinal disorder in a large New Zealand family with a novel mutation in CACNA1F, the gene responsible for CSNB2. Clinical and Experimental Ophthalmology 2005;33:129–136. [PubMed: 15807819]

Jalkanen R, Mantyjarvi M, Tobias R, Alitalo T, Bech-Hansen NT. X-linked cone–rod dystrophy (COD4) in a Finnish family is caused by mutation in CACNA1F. American Journal of Human Genetics 2004;75:A2593.

Jeon CJ, Strettoi E, Masland RH. The major cell populations of the mouse retina. Journal of Neuroscience 1998;18:8936–8946. [PubMed: 9786999]

Kofuji P, Ceelen P, Zahs KR, Surbeck LW, Lester HA, Newman EA. Genetic inactivation of an inwardly rectifying potassium channel (Kir4.1 subunit) in mice: Phenotypic impact in retina. Journal of Neuroscience 2000;20:5733–5740. [PubMed: 10908613]

Koschak A, Reimer D, Walter D, Hoda JC, Heinzle T, Grabner M, Striessnig J. Cav1.4 α_1 subunits can form slowly inactivating dihydropyridine-sensitive L-type Ca^{2+} channels lacking Ca^{2+}-dependent inactivation. Journal of Neuroscience 2003;23:6041–6049. [PubMed: 12853422]

Lamb TD. Ida Mann Lecture. Transduction in human photoreceptors. Australian and New Zealand Journal of Ophthalmology 1996;24:105–110. [PubMed: 9199739]

Li C, Cheng M, Yang H, Peachey NS, Naash MI. Age-related changes in the mouse outer retina. Optometry and Vision Science 2001;78:425–430. [PubMed: 11444632]

Maletic-Savatic M, Malinow R, Svoboda K. Rapid dendritic morphogenesis in CA1 hippocampal dendrites induced by synaptic activity. Science 1999;283:1923–1927. [PubMed: 10082466]

Mansergh F, Orton NC, Vessey JP, Lalonde MR, Stell WK, Tremblay F, Barnes S, Rancourt DE, Hansen NT. Mutation of the calcium channel gene *Cacna1f* disrupts calcium signaling, synaptic transmission and cellular organization in mouse retina. Human Molecular Genetics 2005;14:3035–3046. [PubMed: 16155113]

Massey SC. Cell types using glutamate as a neurotransmitter in the vertebrate retina. Progress in Retinal Research 1990;9:399–425.

Masu M, Iwakabe H, Tagawa Y, Miyoshi T, Yamashita M, Fukuda Y, Sasaki H, Hiroi K, Nakamura Y, Shigemoto R, Takada M, Nakamura K, Nakao K, Katsuki M, Nakanishi S. Specific deficit of the ON response in visual transmission by targeted disruption of the mGluR6 gene. Cell 1995;80:757–765. [PubMed: 7889569]

McCall MA, Lukasiewicz PD, Gregg RG, Peachey NS. Elimination of the ρ_1 subunit abolishes GABA (C) receptor expression and alters visual processing in the mouse retina. Journal of Neuroscience 2002;22:4163–4174. [PubMed: 12019334]

McRory J, Hamid J, Doering C, Garcia E, Parker R, Hamming K, Chen L, Hildebrand M, Beedle A, Feldcamp L, Zamponi G, Snutch T. The CACNA1F gene encodes an L-type calcium channel with unique biophysical properties and tissue distribution. Journal of Neuroscience 2004;24:1707–1718. [PubMed: 14973233]

Miyake Y, Yagasaki K, Horiguchi M, Kawase Y, Kanda T. Congenital stationary night blindness with negative electroretinogram. A new classification. Archives of Ophthalmology 1986;104:1013–1020. [PubMed: 3488053]

Morgans CW. Calcium channel heterogeneity among cone photoreceptors in the tree shrew retina. European Journal of Neuroscience 1999;11:2989–2993. [PubMed: 10457194]

Morgans CW, Bayley PR, Oesch NW, Ren G, Akileswaran L, Taylor WR. Photoreceptor calcium channels: Insight from night blindness. Visual Neuroscience 2005;22:561–568. [PubMed: 16332266]

Morgans CW, Gaughwin P, Maleszka R. Expression of the α_{1F} calcium channel subunit by photoreceptors in the rat retina. Molecular Vision 2001;7:202–209. [PubMed: 11526344]

Mumm JS, Godinho L, Morgan JL, Oakley DM, Schroeter EH, Wong RO. Laminar circuit formation in the vertebrate retina. Progress in Brain Research 2005;147:155–169. [PubMed: 15581704]

Nachman-Clewner M, St. Jules R, Townes-Anderson E. L-type calcium channels in the photoreceptor ribbon synapse: Localization and role in plasticity. Journal of Comparative Neurology 1999;415:1–16. [PubMed: 10540354]

Nakamura M, Ito S, Piao C-H, Terasaki H, Miyake Y. Retinal and optic disc atrophy associated with a CACNA1F mutation in a Japanese family. Archives of Ophthalmology 2003;121:1028–1033. [PubMed: 12860808]

Nusinowitz S, Nguyen L, Radu R, Kashani Z, Farber D, Danciger M. Electroretinographic evidence for altered phototransduction gain and slowed recovery from photobleaches in albino mice with a MET450 variant in RPE65. Experimental Eye Research 2003;77:627–638. [PubMed: 14550405]

Pardue, MT.; Ball, SL.; Candille, SI.; McCall, MA.; Gregg, RG.; Peachey, NS. *nob*: A mouse model of CSNB1. In: Anderson, RE.; LaVail, MM.; Hollyfield, JG., editors. New Insights Into Retinal Degenerative Diseases. Kluwer Academic/Plenum; New York: 2001. p. 319-328.

Pardue MT, McCall MA, LaVail MM, Gregg RG, Peachey NS. A naturally-occurring mouse model of X-linked congenital stationary night blindness. Investigative Ophthalmology and Visual Science 1998;39:2443–2449. [PubMed: 9804152]

Passafaro M, Nakagawa T, Sala C, Sheng M. Induction of dendritic spines by an extracellular domain of AMPA receptor subunit GluR2. Nature 2003;424:677–681. [PubMed: 12904794]

Peichl L, González-Soriano J. Morphological types of horizontal cell in rodent retinae: A comparison of rat, mouse, gerbil, and guinea pig. Visual Neuroscience 1994;11:501–517. [PubMed: 8038125]

Pugh EN Jr. Lamb TD. Amplification and kinetics of the activation steps in phototransduction. Biochimica Biophysica Acta 1993;1141:111–149.

Redburn DA, Rowe-Rendleman C. Developmental neurotransmitters. Signals for shaping neuronal circuitry. Investigative Ophthalmology and Visual Science 1996;37:1479–1482. [PubMed: 8675389]

Robson JG, Frishman LJ. Response linearity and kinetics of the cat retina: The bipolar cell component of the dark-adapted electroretinogram. Visual Neuroscience 1995;12:837–850. [PubMed: 8924408]

Robson JG, Frishman LJ. Dissecting the dark-adapted electroretinogram. Documenta Ophthalmologica 1998;95:187–215. [PubMed: 10532405]

Rosen LB, Ginty DD, Weber MJ, Greenberg ME. Membrane depolarization and calcium influx stimulate MEK and MAP kinase via activation of Ras. Neuron 1994;12:1207–1221. [PubMed: 8011335]

Sagdullaev BT, DeMarco PJ, McCall MA. Improved contact lens electrode for corneal ERG recordings in mice. Documenta Ophthalmologica 2004;108:181–184. [PubMed: 15573941]

Sagdullaev BT, McCall MA. Stimulus size and intensity alter fundamental response properties of mouse retinal ganglion cells in vivo. Visual Neuroscience 2005;22:649–659. [PubMed: 16332276]

Schmitz F, Konigstorfer A, Sudhof TC. RIBEYE, a component of synaptic ribbons: A protein's journey through evolution provides insight into synaptic ribbon function. Neuron 2000;28:857–872. [PubMed: 11163272]

Schmitz Y, Witkovsky P. Dependence of photoreceptor glutamate release on a dihydropyridine-sensitive Ca^{2+} channel. Neuroscience 1997;78:1209–1216. [PubMed: 9174087]

Sharma S, Ball SL, Peachey NS. Pharmacological studies of the mouse cone electroretinogram. Visual Neuroscience 2005;22:631–636. [PubMed: 16332274]

Sieving PA, Murayama K, Naarendorp F. Push–pull model of the primate photopic electroretinogram: A role for hyperpolarizing neurons in shaping the *b*-wave. Visual Neuroscience 1994;11:519–532. [PubMed: 8038126]

Sterling P, Matthews G. Structure and function of ribbon synapses. TINS 2005;28:20–29. [PubMed: 15626493]

Strom TM, Nyakatura G, Apfelstedt-Sylla E, Hellebrand H, Lorenz B, Weber BH, Wutz K, Gutwillinger N, Rüther K, Drescher B, Sauer C, Zrenner E, Meitinger T, Rosenthal A, Meindl A. An L-type calcium-channel gene mutated in incomplete X-linked congenital stationary night blindness. Nature Genetics 1998;19:260–263. [PubMed: 9662399]

Tagawa Y, Sawai H, Ueda Y, Tauchi M, Nakanishi S. Immunohistological studies of metabotropic glutamate receptor subtype 6-deficient mice show no abnormality of retinal cell organization and ganglion cell maturation. Journal of Neuroscience 1999;19:2568–2579. [PubMed: 10087070]

Taylor BA, Navin A, Phillips SJ. PCR-amplification of simple sequence repeat variants from pooled DNA samples for rapidly mapping new mutations of the mouse. Genomics 1994;21:626–632. [PubMed: 7959741]

Taylor WR, Morgans C. Localization and properties of voltage-gated calcium channels in cone photoreceptors of *Tupaia belangeri*. Visual Neuroscience 1998;15:541–552. [PubMed: 9685206]

tom Dieck S, Altrock WD, Kessels MM, Qualmann B, Regus H, Brauner D, Fejtová A, Bracko O, Gundelfinger ED, Brandstätter JH. Molecular dissection of the photoreceptor ribbon synapse: Physical interaction of Bassoon and RIBEYE is essential for the assembly of the ribbon complex. Journal of Cell Biology 2005;168:825–836. [PubMed: 15728193]

von Gersdorff H. Synaptic ribbons: Versatile signal transducers. Neuron 2001;29:7–10. [PubMed: 11182076]

Wachtmeister L. Oscillatory potentials in the retina: What do they reveal. Progress in Retinal and Eye Research 1998;17:485–521. [PubMed: 9777648]

Wilkinson MF, Barnes S. The dihydropyridine-sensitive calcium channel subtype in cone photoreceptors. Journal of General Physiology 1996;107:621–630. [PubMed: 8740375]

Wollstein G, Paunescu LA, Ko TH, Fujimoto JG, Kowalevicz A, Hartl I, Beaton S, Ishikawa H, Mattox C, Singh O, Duker J, Drexler W, Schuman JS. Ultrahigh-resolution optical coherence tomography in glaucoma. Ophthalmology 2005;112:229–237. [PubMed: 15691556]

Wong WT, Faulkner-Jones BE, Sanes JR, Wong RO. Rapid dendritic remodeling in the developing retina: Dependence on neurotransmission and reciprocal regulation by Rac and Rho. Journal of Neuroscience 2000;20:5024–5036. [PubMed: 10864960]

Wong WT, Wong RO. Changing specificity of neurotransmitter regulation of rapid dendritic remodeling during synaptogenesis. Nature Neuroscience 2001;4:351–352.

Wutz K, Sauer C, Zrenner E, Lorenz B, Alitalo T, Broghammer M, Hergersberg M, de la Chapelle A, Weber BH, Wissinger B, Meindl A, Pusch CM. Thirty distinct *CACNA1F* mutations in 33 families with incomplete type of XLCSNB and *Cacna1f* expression profiling in mouse retina. European Journal of Human Genetics 2002;10:449–456. [PubMed: 12111638]

Yang XL. Characterization of receptors for glutamate and GABA in retinal neurons. Progress in Neurobiology 2004;73:127–150. [PubMed: 15201037]

Zeitz C, Minotti R, Feil S, Mátyás G, Cremers FPM, Hoyng CB, Berger W. Novel mutations in *CACNA1F* and *NYX* in Dutch families with X-linked congenital stationary night blindness. Molecular Vision 2005;11:179–183. [PubMed: 15761389]

Zhang N, Townes-Anderson E. Regulation of structural plasticity by different channel types in rod and cone photoreceptors. Journal of Neuroscience 2002;22:7065–7079. [PubMed: 12177203]

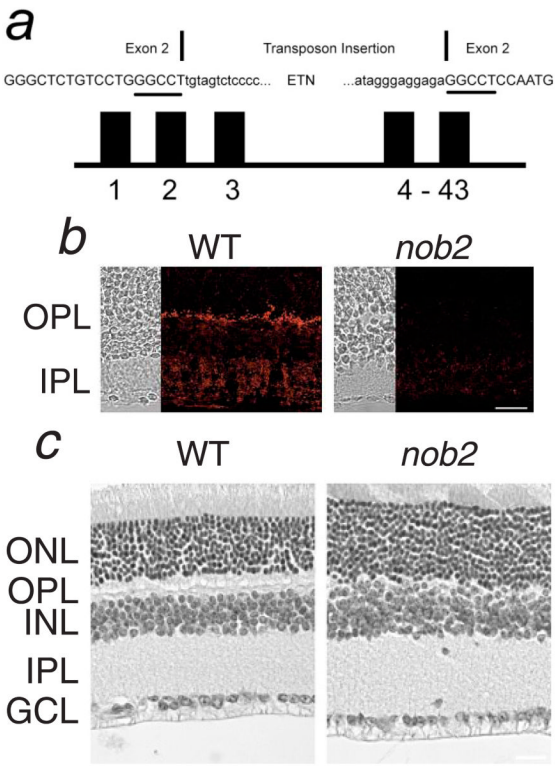

Fig. 1.

(a) Diagram of *Cacna1f*, indicating the location of the intragenic insertion into exon 2. Exon 2 nucleotides are shown as capitals. The 6-bp duplication at the insertion site is underlined. (b) Immunofluorescent staining for α_{1F} is localized to the OPL and the IPL of the WT retina but is absent in the *nob2* retina. (c) Comparison of retinal anatomy in adult WT and *nob2* mice. In the *nob2* retina, the OPL is disorganized but other retinal layers appear normal. GCL, ganglion cell layer; IPL, inner plexiform layer INL, inner nuclear layer; OPL, outer plexiform layer; and ONL, outer nuclear layer. Scale bar indicates 20 μm (b) or 40 μm (c).

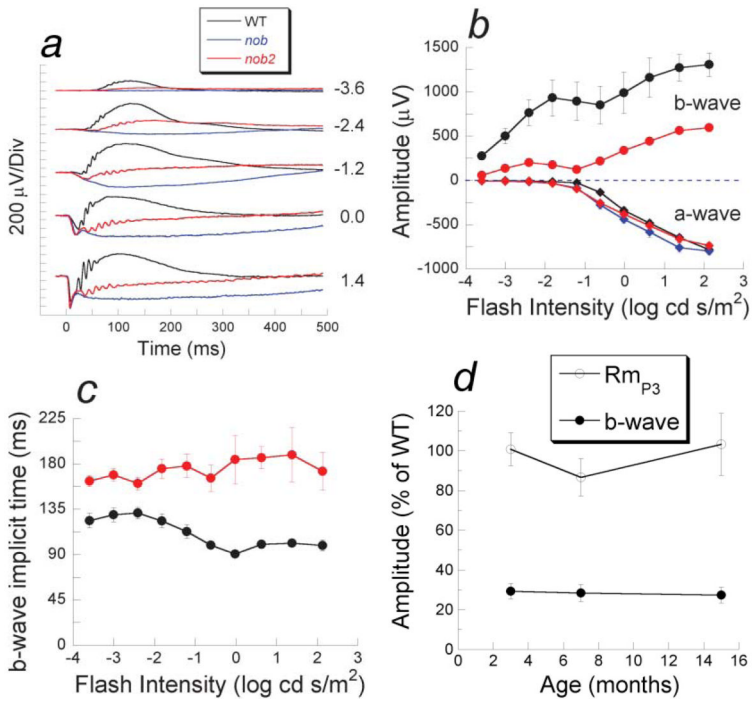

Fig. 2.

Dark-adapted electroretinograms. (a) Comparison of dark-adapted ERGs recorded from *nob2* mice (red tracings) with those obtained from WT (black tracings) or *nob* (blue tracings) mice. Numbers indicate flash intensity in log cd s/m^2. (b) Amplitude of the dark-adapted *a*-wave (diamonds) or *b*-wave (circles) for *nob2* (red), *nob* (blue), and WT (black) mice. Data points indicate the mean ± S.E.M. response for four mice tested at 6 weeks of age. (c) *b*-wave implicit times of *nob2* (red circles) and WT (black circles) mice. Data points in (b & c) indicate the mean ± S.E.M. response for four *nob2* or WT mice, tested at 6 weeks of age. (d) Relative amplitude of *a*-wave parameter Rm_{P3} (open circles) or *b*-wave amplitude obtained to a 0.3 log cd s/m^2 stimulus (filled circles) plotted as a function of age for *nob2* mice relative to the WT mean. Data points in (d) indicate the mean ± S.E.M. Response for 5–7 *nob2* mice, which are expressed relative to the mean value obtained from 9–10 WT mice.

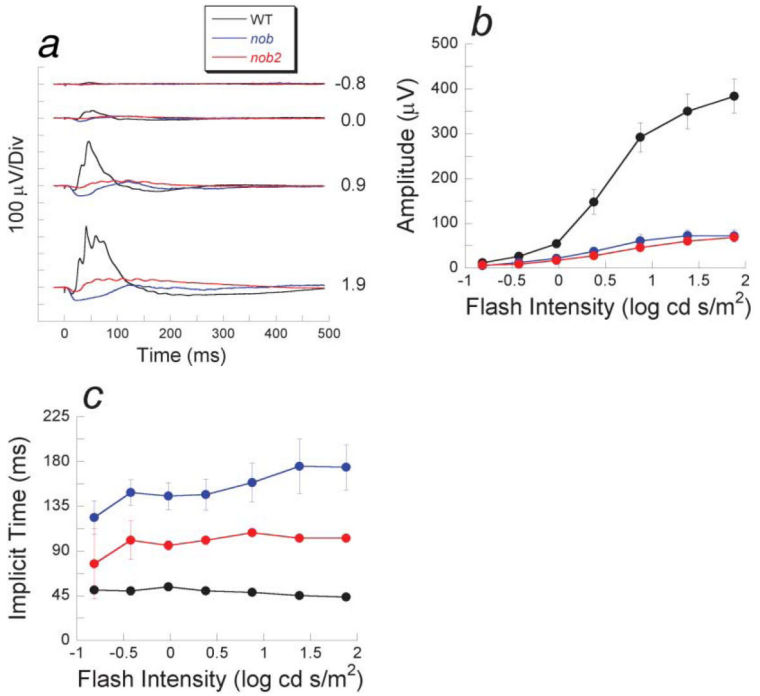

Fig. 3.

Light-adapted electroretinograms. (a) Comparison of ERGs recorded from *nob2* mice (red tracings) with those obtained from WT (black tracings) or *nob* (blue tracings) mice. Numbers indicate flash intensity in log cd s/m^2. Amplitude (b) and implicit time(c) of the cone ERG *b*-wave for *nob2* (red circles), *nob* (blue circles) and WT (black circles) mice. Data points in (b &c) indicate the mean ± S.E.M. response for four mice tested at 6 weeks of age.

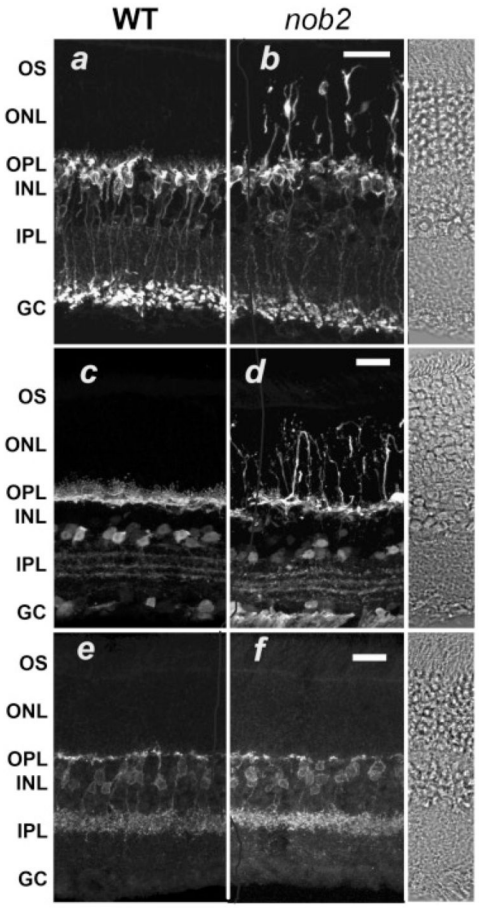

Fig. 4.

Bipolar and horizontal cells extend dendritic processes into the ONL in the *nob2* but not WT retina. Retinal sections from WT (a, c, & e) or *nob2* (b, d, & f) retinas immunolabeled with antibodies against the rod bipolar cell marker, PKCα (a & b), the horizontal cell marker, calbindin (c & d), or the HBC marker NK3R (e &f). INL, inner nuclear layer; OPL, outer plexiform layer; and ONL, outer nuclear layer. DIC images were obtained from a WT retina. Scale bar indicates 20 μm. Mice were studied at 5 months of age.

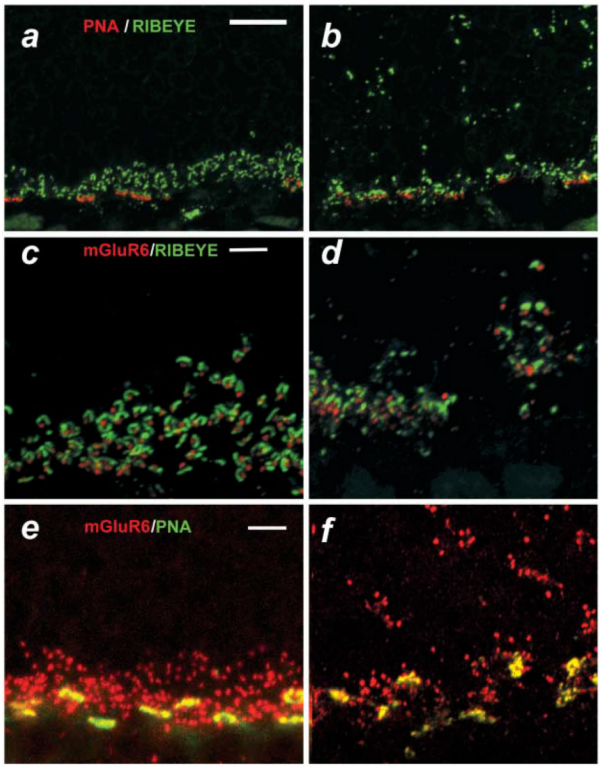

Fig. 5.

Synaptic abnormalities in *nob2* retina. (a–f) micrographs of vertical sections through WT (a, c, & e) or *nob2* (b, d, & f) retinas immunolabeled with PNA (red)/Ribeye (green; [a & b]), mGluR6 (red)/Ribeye (green; [c & d] or mGluR6 (red)/PNA (green; [e & f]. Scale bar indicates 10 μm (a, b) or 5 μm (c–f). Mice were studied at 5 months of age.

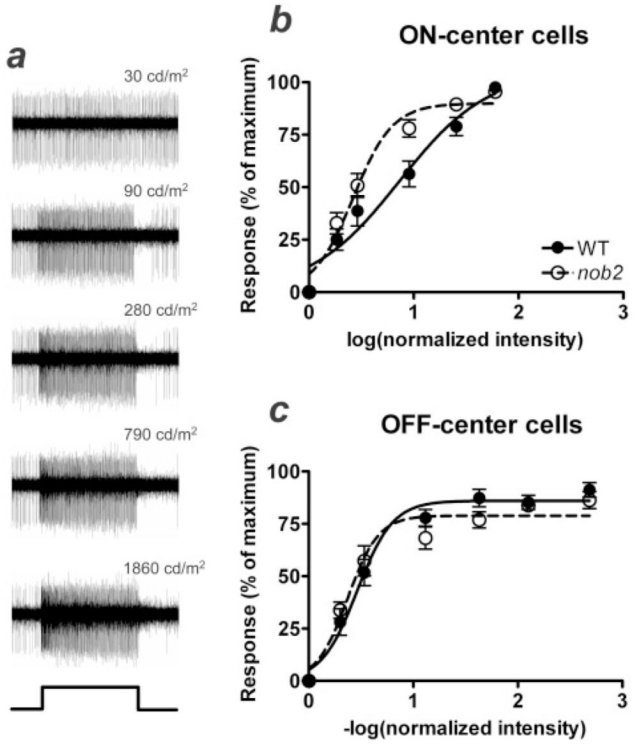

Fig. 6.

Ganglion cell responses in *nob2* mice. Representative raw traces from an ON-center RGC in a *nob2* mouse are shown in (a) and were obtained by recording from the optic nerve *in vivo*. The cell's response to the 30 cd/m2 adapting background is shown at the top and the responses to increasing intensity spot stimuli from 90 cd/m^2 to 1860 cd/m^2 are shown from top to bottom. A profile of the stimulus is shown at the bottom of the column. Intensity–response functions are shown in (b) for ON- and (c) for OFF-center RGCs for *nob2* and WT animals. Responses are plotted as the mean spike rate (spikes/s) determined for the first 0.5 s of the stimulus, expressed as a percentage of the maximum response obtained for that cell. Responses are plotted against the log (normalized intensity) for ON-center cells and −log (normalized intensity) for OFF-center cells), as defined in the Methods. Data points indicate mean ± S.E.M. for 16 WT ON-center cells, 13 *nob2* ON-center cells, 11 WT OFF-center cells, or 11 *nob2* OFF-center cells. Curves represent the Hill equation fitted to the averaged data set, to derive the semisaturation constant and slope. Mice were studied at 5 months of age.

Table 1

Stimulus intensities and interstimulus intervals used for RGC intensity–response functions

Interstimulus interval (s)	Intensity (cd/m^2) ON-center cells	Intensity (cd/m^2) OFF-center cells
10		7.95
15	54	2.7
20	90	0.7
40	280	0.26
60	789	0.088
	1860	0.028